Phytophthora infestans effector AVRblb2 prevents secretion of a plant immune protease at the haustorial interface

Tolga O. Bozkurt[a,1], Sebastian Schornack[a,1], Joe Win[a], Takayuki Shindo[b], Muhammad Ilyas[b], Ricardo Oliva[a], Liliana M. Cano[a], Alexandra M. E. Jones[a], Edgar Huitema[a,2], Renier A. L. van der Hoorn[b], and Sophien Kamoun[a,3]

[a]The Sainsbury Laboratory, Norwich Research Park, Norwich NR4 7UH, United Kingdom; and [b]Plant Chemetics Laboratory, Max Planck Institute for Plant Breeding Research, 50829 Cologne, Germany

Edited by Brian J. Staskawicz, University of California, Berkeley, CA, and approved November 10, 2011 (received for review August 4, 2011)

In response to pathogen attack, plant cells secrete antimicrobial molecules at the site of infection. However, how plant pathogens interfere with defense-related focal secretion remains poorly known. Here we show that the host-translocated RXLR-type effector protein AVRblb2 of the Irish potato famine pathogen *Phytophthora infestans* focally accumulates around haustoria, specialized infection structures that form inside plant cells, and promotes virulence by interfering with the execution of host defenses. AVRblb2 significantly enhances susceptibility of host plants to *P. infestans* by targeting the host papain-like cysteine protease C14 and specifically preventing its secretion into the apoplast. Plants altered in C14 expression were significantly affected in susceptibility to *P. infestans* in a manner consistent with a positive role of C14 in plant immunity. Our findings point to a unique counterdefense strategy that plant pathogens use to neutralize secreted host defense proteases. Effectors, such as AVRblb2, can be used as molecular probes to dissect focal immune responses at pathogen penetration sites.

plant cell-autonomous immunity | polarized secretion | late blight

To enable parasitism and symbiosis, plant-associated organisms intimately interact with plant cells often through specialized cellular structures. Some biotrophic fungal and oomycete pathogens form accommodation structures termed haustoria that invaginate the host cell plasma membrane to deliver pathogenicity effector proteins and acquire nutrients (1, 2). In response to and to restrict pathogen colonization, the attacked plant cell undergoes significant cellular reorganization, involving organelle relocation, cell-wall reinforcements around contact sites, and polarized secretion of antimicrobial molecules (3, 4).

An important group of host-secreted defense components are papain-like cysteine proteases (PLCPs). As a countermeasure, effective pathogens such as *Phytophthora infestans*, the oomycete pathogen that causes potato late blight, secrete extracellular protease inhibitors of cysteine proteases (EPICs) that bind and inhibit PLCPs in the apoplast (5). The existence of protease inhibitors from unrelated pathogens, such as *Cladosporium fulvum* Avr2 and *P. infestans* cystatin-like EPIC2B, that both target and inhibit apoplastic PLCPs RCR3 and PIP1 of tomato points to a key role of this group of proteases in immunity (6). Furthermore, a secreted PLCP RD19 from *Arabidopsis* is targeted and mislocalized to the host cell nucleus by the bacterial type III secreted effector PopP2 from *Ralstonia solanacearum* (7). Given the importance of apoplastic host defenses, it is likely that *P. infestans* has established multiple strategies to counteract secreted defense components, potentially including direct targeting of elements of the polarized secretion pathway.

The *P. infestans* genome encodes large families of host-translocated effectors (8, 9). The best-studied group of *P. infestans* effectors is the RXLR effector family, named for the presence of a conserved arginine-X-leucine-arginine motif. RXLR effectors operate inside the host cell to enable successful infection. Similar to other RXLR effectors, AVRblb2 ($PexRD40_{170–7}$) (10) is a modular protein with the N-terminal half comprising a signal peptide and the RXLR domain involved in trafficking to host cell cytoplasm and the C-terminal region carrying the biochemical effector activities (10). As noted for other RXLR effectors with avirulence activity, *Avrblb2* and its paralogs are sharply up-regulated during infection, peaking early during biotrophy (8, 10). These genes are important for *P. infestans* fitness because every known strain of the pathogen carries multiple intact coding sequences (10). Members of the AVRblb2 family are recognized inside plant cells by the broad-spectrum resistance protein Rpiblb2 of the wild potato *Solanum bulbocastanum* (10). However, the primary activity of AVRblb2 and other RXLR effectors is to promote virulence, and the precise modes of action and host targets of these effectors remain largely unknown (11). Only recently, the RXLR effector AVR3a was shown to manipulate plant immunity by stabilizing the host E3 ligase CMPG1 (12). However, the extent to which plant pathogen effectors interfere with defense-related focal secretion is poorly known.

Here we show that the host-translocated RXLR-type effector protein AVRblb2 of the Irish potato famine pathogen *P. infestans* focally accumulates around haustoria inside plant cells and promotes virulence by interfering with the execution of polarized host defenses. Furthermore, we demonstrate that AVRblb2 targets PLCP C14 and prevents its secretion into the apoplast. C14 knockdown via RNAi-mediated silencing results in enhanced susceptibility toward *P. infestans* and promotes its hyphal growth. We present evidence that C14 is a unique plant defense protease and its overexpression limits *P. infestans* infection efficiency. However, this effect is partially reversed by *in planta* overexpression of AVRblb2. Our data point to a unique counterdefense strategy that plant pathogens use to neutralize secreted plant defense proteases. Effectors, such as AVRblb2, can be used as molecular probes to dissect focal immune responses at pathogen penetration sites.

Results and Discussion

AVRblb2 Localizes to the Cell Periphery and Accumulates Around Haustoria in Infected Cells. To gain insight into AVRblb2 virulence activities inside host cells, we constructed a functional N-

Author contributions: T.O.B., S.S., J.W., A.M.E.J., E.H., R.A.L.v.d.H., and S.K. designed research; T.O.B., S.S., J.W., T.S., M.I., and R.O. performed research; T.O.B., S.S., J.W., L.M.C., A.M.E.J., R.A.L.v.d.H., and S.K. analyzed data; and T.O.B., S.S., and S.K. wrote the paper.

The authors declare no conflict of interest.

This article is a PNAS Direct Submission.

[1]T.O.B. and S.S. contributed equally to this work.

[2]Present address: Division of Plant Sciences, College of Life Sciences, University of Dundee, Dundee DD2 5DA, United Kingdom.

[3]To whom correspondence should be addressed. E-mail: sophien.kamoun@tsl.ac.uk.

This article contains supporting information online at www.pnas.org/lookup/suppl/doi:10.1073/pnas.1112708109/-/DCSupplemental.

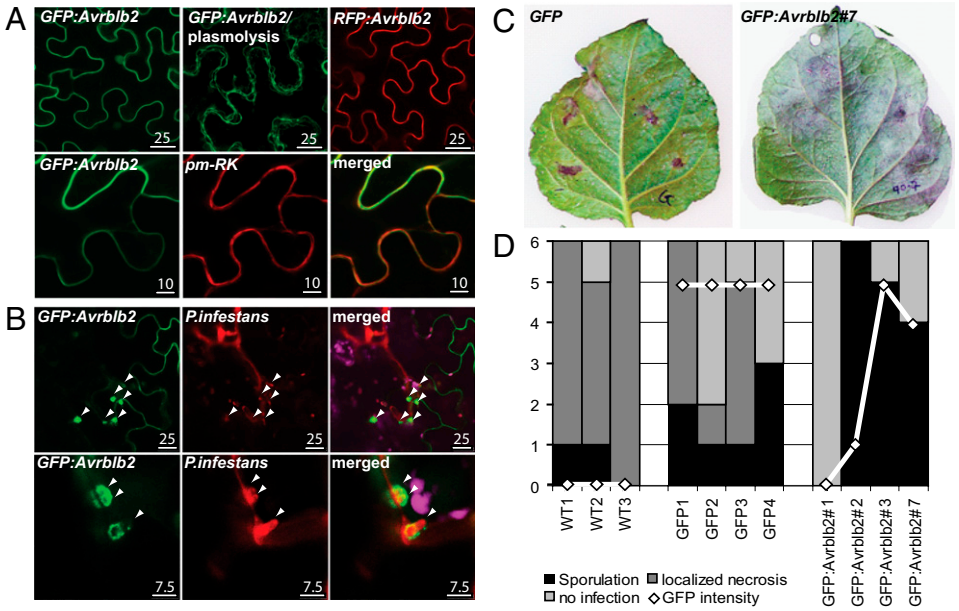

Fig. 1. AVRblb2 localizes to the plasma membrane and accumulates around haustoria to promote *P. infestans* virulence. (*A*) *Agrobacterium tumefaciens*-mediated transient expression of GFP:AVRblb2 or RFP:AVRblb2 fusion proteins revealed peripheral localization, which was not affected by plasmolysis and overlapped with a plasma membrane marker (pm-RK). (*B*) *P. infestans*-infected cells (red) focally accumulated GFP:AVRblb2 (green) around haustoria (arrowheads). Magenta represents the signal from plastids. (*C*) *GFP:Avrblb2* transgenic *N. benthamiana* plants (5 wk old) were more susceptible to infection and enabled faster *P. infestans* sporulation compared with controls. (*D*) Quantitative scoring of infection stages and GFP expression intensities on WT, control (*GFP*), and *GFP:Avrblb2* transgenic lines. The *x* axis represents the position on the intensity transect, and the white line represents GFP signal intensities of transgenic lines. The *y* axis depicts the number of successful infections (each leaf is inoculated with *Phytophthora* at six different spots).

terminal GFP fusion to mature AVRblb2 (lacking the signal peptide) (Fig. S1 *A* and *B*). The GFP:AVRblb2 fusion protein accumulated mainly at the cell periphery when expressed in *Nicotiana benthamiana* (Fig. 1*A*). The fluorescence signal remained associated with the plasma membrane after salt-induced plasmolysis of the epidermal cells (Fig. 1*A*). The AVRblb2 signal largely overlapped with the red fluorescence of a coexpressed plasma membrane-localized RFP (pm-RK), confirming that AVRblb2 accumulates at the host plasma membrane (Fig. 1*A*). Similar membrane localization of AVRblb2 was observed with an N-terminal RFP fusion (Fig. 1*A*) and in stable transgenic *GFP:AVRblb2* lines of *N. benthamiana* (Fig. S1*C*). To determine the extent to which localization of AVRblb2 is altered during infection, we inoculated the *GFP:AVRblb2 N. benthamiana* lines

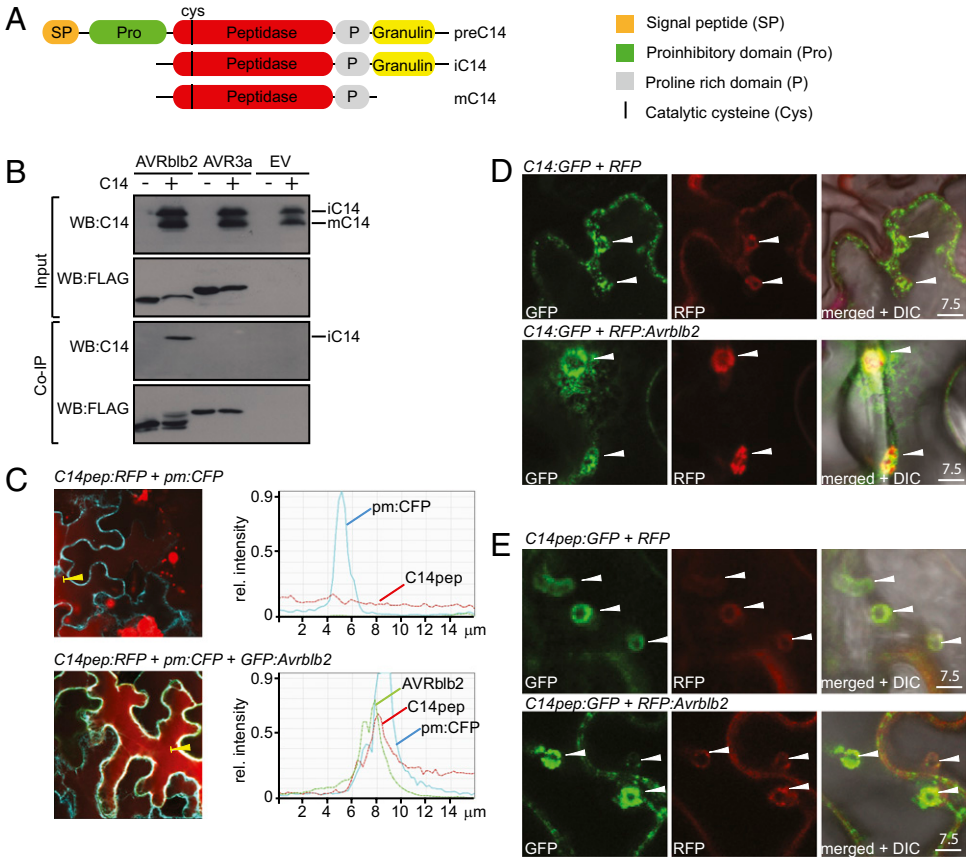

Fig. 2. AVRblb2 associates with C14 *in planta*. (*A*) Domain organization of C14. C14 accumulates in cells as immature (iC14) and mature (mC14) isoforms. (*B*) AVRblb2 coimmunoprecipitates with C14 *in planta*. *FLAG:Avrblb2* or *FLAG:Avr3a* was transiently coexpressed alone or with C14 in *N. benthamiana*. Immunoprecipitates obtained with anti-FLAG antiserum and total protein extracts were immunoblotted with appropriate antisera. (*C*) C14pep:RFP was detected in vacuoles and as apoplastic aggregates, which did not colocalize with plasma membrane CFP (pm:CFP; *Upper*). Coexpression of *GFP:Avrblb2* increased C14pep:RFP intensity at the plasma membrane (*Lower*). Fluorescence intensities of CFP/GFP/RFP in membrane transects (yellow arrowheads) at 3 d postinfiltration (dpi) are illustrated. (*D* and *E*) C14:GFP (*D*) and C14pep:GFP (*E*) accumulate at haustorial sites (arrowheads). Accumulation was enhanced upon *RFP:Avrblb2* coexpression. Pictures were taken at 3 d post infection (*D*) and 4 d post infection (*E*).

PLANT BIOLOGY

with several *P. infestans* strains, including 88069td, a transgenic strain expressing the red fluorescent marker tandem dimer RFP (known as tdTomato) (13). The AVRblb2 signal preferentially accumulated around haustoria inside infected plant cells, whereas its even distribution at the plasma membrane remained unaltered in cells without haustoria (Fig. 1*B*). Haustorial accumulation of AVRblb2 first occurred at discrete focal sites (one per haustorium) before covering the entire surface of the haustoria (Fig. 1*B* and Fig. S1*C*). Perihaustorial accumulation of AVRblb2 only partially overlapped with callose deposited around haustoria and was not associated with callose encasements (Fig. S1*D*) (14).

AVRblb2 Enhances *P. infestans* Virulence. To determine the degree to which AVRblb2 affects *P. infestans* infection, we performed pathogen assays with the transgenic *GFP:AVRblb2 N. benthamiana* plants. The *GFP:AVRblb2* plants showed enhanced susceptibility to *P. infestans*, resulting in increased pathogen colonization and sporulation relative to control lines (Fig. 1 *C* and *D* and Fig. S2). This finding indicates that AVRblb2 has a virulence activity and suggests that it causes significant impairment of host defense responses.

AVRblb2 Associates with C14 Protease *in Planta*. To identify the host targets of AVRblb2, we used *in planta* coimmunoprecipitation (co-IP) followed by liquid chromatography–tandem mass spectrometry (LC-MS/MS). In total, we detected five *N. benthamiana* proteins that specifically associated with AVRblb2 (Table S1). One of these targets is the PLCP C14, a conserved solanaceous protein orthologous to *Arabidopsis* RD21, rice Oryzain, and maize Mir3 cysteine proteases (15–20). C14 is a complex modular protein featuring a predicted N-terminal secretion signal and a self-inhibitory prodomain, which is followed by peptidase, proline-rich, and granulin domains (Fig. 2*A*). In plant cells, C14/RD21 converts into immature (iC14) and mature (mC14) isoforms (Fig. 2*A*) that accumulate into various subcellular compartments and the apoplast (16–18). C14 and other PLCPs have been implicated in plant immunity, including pathogen perception and disease resistance (5, 21). Like some other PLCPs, C14 is also targeted by apoplastic protease inhibitor effectors of *P. infestans* and other filamentous pathogens (5, 6, 18), and the expression of the potato *C14* gene is rapidly induced during *P. infestans* infection (15). Thus, we decided to initially focus on C14, and we will study other AVRblb2-associated proteins in the future.

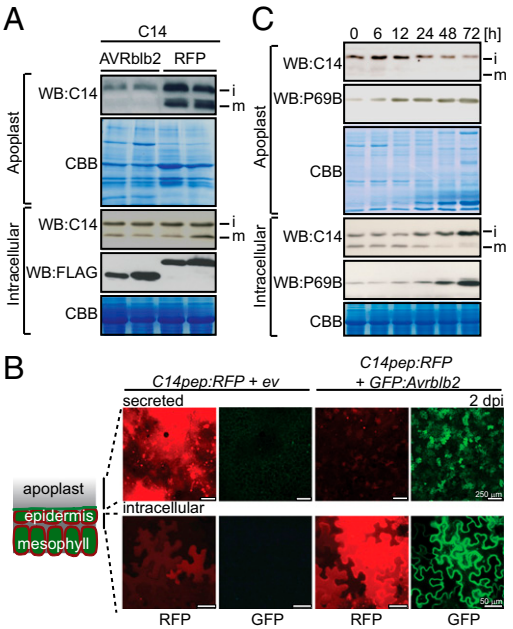

Fig. 3. AVRblb2 inhibits secretion of C14. (*A*) *FLAG:Avrblb2* or *FLAG:RFP* was transiently coexpressed with *C14* in *N. benthamiana* (two biological replicates for both *FLAG:AVRblb2* and *FLAG:RFP* were used). Apoplastic and intracellular leaf extracts were separated and stained with Coomassie Brilliant Blue (CBB). Immunoblots with appropriate antisera showed reduced apoplastic iC14 (i) and mC14 (m) levels. (*B*) Confocal sectioning of epidermal cells revealed that apoplastic accumulation of C14pep:RFP (*Upper*) was reduced and shifted to intracellular vacuoles (*Lower*) upon transient coexpression with *GFP:Avrblb2*. (*C*) *P. infestans* colonization of tomato is associated with a decrease in apoplastic C14. Apoplastic or intracellular C14 and P69B protein levels were assessed from infected tomato leaves over a time course. Immunoblotting of apoplastic fluids and intracellular protein extracts showed a marked reduction of apoplastic C14 levels starting at 24 h after inoculation, whereas intracellular iC14 levels increased. In contrast, a significant increase in both apoplastic and intracellular P69B levels were observed.

We validated the specific *in planta* association between AVRblb2 and tomato C14 (LeC14) with co-IP (Fig. 2*B*). AVRblb2-purified immunocomplexes contained iC14 (Fig. 2*B*), and, occasionally, the less abundant mC14 isoform of the protease could be detected (Fig. S3). We next addressed whether C14 associates with AVRblb2 *in planta* by using confocal microscopy. As previously reported for the C14 ortholog RD21 (16, 17), fluorescently tagged full-length C14 and a C14 construct lacking the granulin domain (C14pep) localized to the endoplasmic reticulum (ER), endomembrane compartments, vacuoles, and apoplast (Fig. 2*C* and Fig. S4 *B*–*E*) and accumulated around haustoria in infected cells (Fig. S4*F*). Notably, in the presence of AVRblb2, the localization of C14 dramatically shifted toward the cell periphery, resulting in a marked overlap with the fluorescence signals of AVRblb2 and a plasma membrane marker (Fig. 2*C* and Fig. S5*A*). A similar shift in C14 distribution was observed in plant cells containing haustoria (haustoriated plant cells), resulting in colocalization and focal accumulation of AVRblb2 and C14 around haustoria (Fig. 2*D*). Altogether, these results indicate that AVRblb2 associates with C14 and alters its subcellular distribution.

AVRblb2 Prevents Secretion of the C14 Protease. The increased peripheral accumulation of C14 triggered by AVRblb2 prompted us to address whether AVRblb2 affects secretion of C14. AVRblb2 significantly reduced apoplastic levels of C14 without affecting its intracellular accumulation (Fig. 3*A* and Fig. S5*B*). AVRblb2 did not inhibit secretion in general because it did not affect secretion of the pathogenesis-related serine protease P69B nor did it reduce overall protein levels in the apoplast (Fig. S5*C*). We confirmed these observations by microscopy. AVRblb2 significantly reduced the apoplastic accumulation of a C14pep:RFP fusion protein but increased its levels in the cytoplasm, mainly in the cell periphery and vacuoles (Fig. 3*B*). In contrast, AVRblb2 did not alter the apoplastic levels of a fusion of basic chitinase signal peptide to GFP (SP:GFP), confirming again that AVRblb2 does not generally prevent secretion (Fig. S5*D*). In summary, these results indicate that AVRblb2 inhibits secretion of the host protease C14.

Consistent with these observations, we noted a gradual decrease in C14 levels in the tomato apoplast during *P. infestans* infection starting at 24 h after inoculation (Fig. 3*C*). Intracellular levels of C14 were also altered during infection with an increase in iC14 levels (Fig. 3*C*). These changes contrast sharply with the well-known increase in apoplastic levels of pathogenesis-related proteins, such as P69B, over the course of infection (Fig. 3*C*) (22). The decrease in apoplastic C14 during infection could be attributable to the preferential targeting of this protein to haustorial sites, where it is prevented from secretion. However,

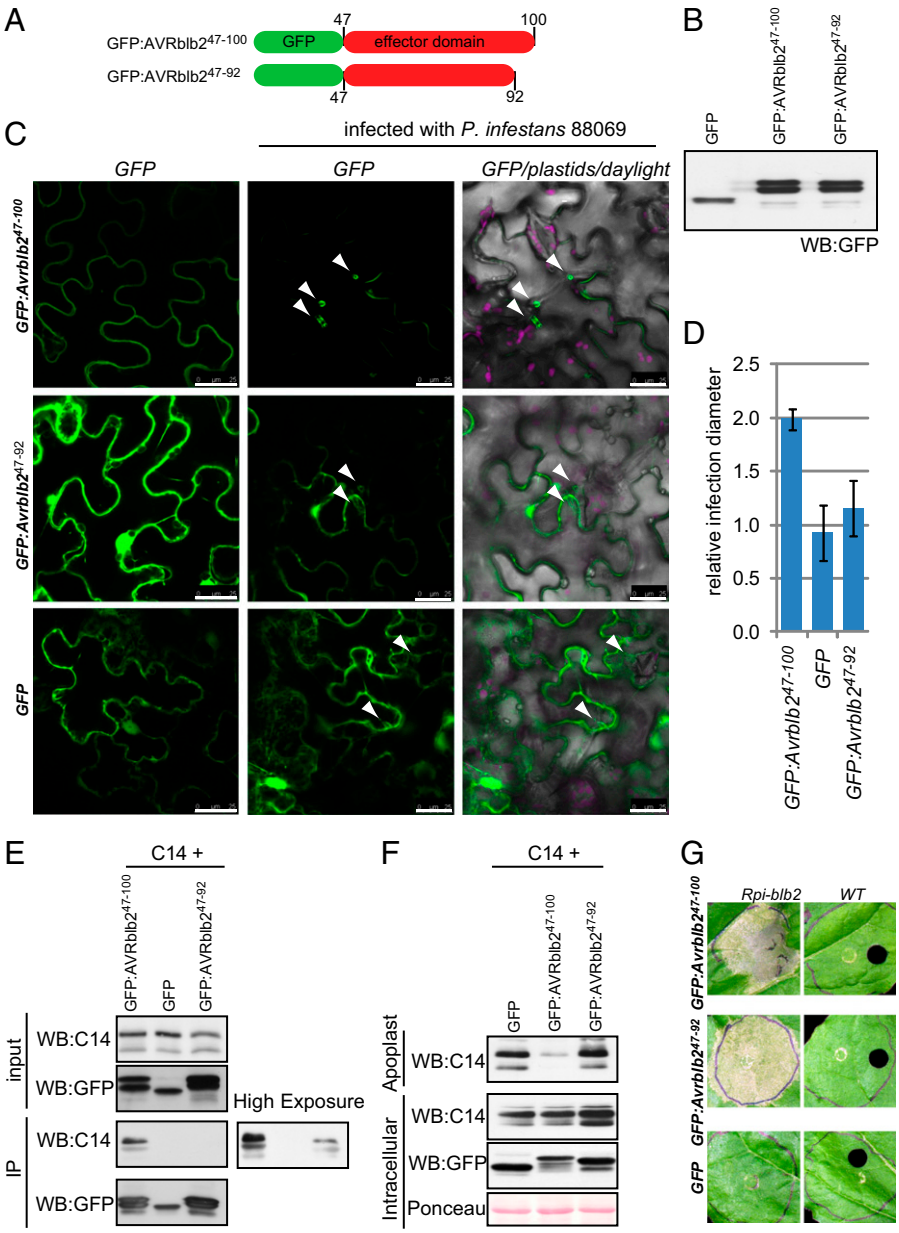

Fig. 4. An AVRblb2 mutant is impaired in haustorial localization and virulence effects but retains avirulence activity. (*A*) Overview of the constructs. The numbers correspond to AVRblb2 full-length protein amino acid residue positions. (*B*) Immunoblots of constructs expressed in *N. benthamiana*. (*C*) GFP:AVRblb2$^{47–100}$ (GFP:AVRblb2) shows localization to the cell periphery in uninfected leaves and focal accumulation around haustoria (arrowheads) in leaves infected with *P. infestans* 88069, whereas the mutant *GFP:AVRblb2*$^{47–92}$ shows a subcellular distribution that resembles GFP (nucleocytoplasmic) and does not focally accumulate at haustoria at 3 d post infection. (Scale bars: 25 μm.) Green color is GFP, and magenta is plastid fluorescence. (*D*) AVRblb2 mutant does not enhance pathogen growth. (*E*) Co-IP of GFP:AVRblb2, GFP:AVRblb2$^{47–92}$, and GFP with C14. (*F*) Levels of apoplastic C14 are reduced by coexpression of AVRblb2 but not by GFP:AVRblb2$^{47–92}$ or GFP. (*G*) *GFP:AVRblb2*$^{47–92}$ retains avirulence activity. *A. tumefaciens*-mediated transient expression of GFP-fused *Avrblb2* constructs or control (GFP) in *Rpi-blb2* transgenic and WT *N. benthamiana*.

based on this experiment, we cannot exclude that the observed effect might involve additional effectors to AVRblb2.

AVRblb2 Localization Is Required for Its Virulence Function. To address the link between AVRblb2 haustorial localization and its function, we tested several deletion mutants and identified an 8-aa C-terminal deletion mutant (AVRblb2$^{47–92}$) that did not exclusively accumulate at the cell periphery or around haustoria (Fig. 4 *A*–*C*). Notably, this mutant lost its ability to enhance *P. infestans* growth (Fig. 4*D*), weakly associated with C14 protease, and failed to attenuate apoplastic C14 accumulation (Fig. 4 *E* and *F*). Thus, localization of AVRblb2 and C14 secretion inhibition are genetically linked to the enhanced virulence activity of this effector. Conversely, the mutant retained its activity to trigger an *Rpi-blb2*–dependent hypersensitive response (Fig. 4*G*). These results indicate that AVRblb2 localization is essential for its virulence function but not for its avirulence activity.

C14 Protease Positively Contributes to Immune Responses Against *P. infestans*. To determine the extent to which C14 contributes to plant immunity, we altered C14 expression in *N. benthamiana*. Stable RNAi *N. benthamiana* lines, carrying two independent C14 hairpin constructs (5), showed significantly enhanced susceptibility to *P. infestans* compared with control lines as assessed

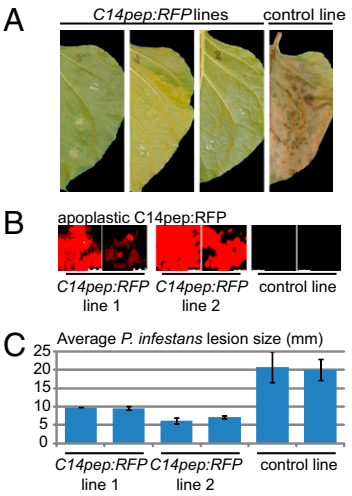

Fig. 5. A positive role for C14 in plant immunity against *P. infestans*. (*A*) Differential growth of *P. infestans* 88069 on tomato *C14pep:RFP*-expressing *N. benthamiana* lines (5 wk old). Pictures were taken at 8 d after infection. (*B*) Leaf apoplastic C14pep:RFP levels in descendants of two independent transgenic *N. benthamiana* lines were measured by using confocal microscopy. (*C*) Plants with apoplastic C14pep:RFP accumulation showed reduced hyphal growth of *P. infestans* 88069 compared with ER-GFP–expressing *control N. benthamiana* lines (5 wk old). Growth efficiency was plotted as average total growing necrosis diameter (n = 6) at 5 d after infection.

by increased disease symptoms (Fig. S6). Conversely, overexpression of both C14 and C14pep in *N. benthamiana* resulted in reduced *P. infestans* colonization relative to controls (Fig. 5 and Fig. S7 *A* and *B*). This enhanced immunity conferred by C14 could be partially reversed by simultaneous overexpression of AVRblb2 (Fig. S7 *C* and *D*). In the course of these experiments, we also determined that *C14* silencing did not affect Rpi-blb2 recognition of AVRblb2, indicating that C14 is not "guarded" by Rpi-blb2 (Fig. S8) (23, 24). These results indicate that C14 plays a positive role in plant immunity. We propose a model in which C14 is targeted by two classes of effectors in separate plant cell compartments: whereas AVRblb2 prevents secretion of C14 within haustoriated plant cells, other *P. infestans* effectors inhibit C14 in the apoplast as shown by Kaschani et al. (5) (Fig. 6).

A Plant Pathogen Effector That Probes Defense-Related Polarized Secretion. In this study, we showed that the *P. infestans* effector AVRblb2 interferes with defense-related secretion in haustoriated plant cells. AVRblb2 can enhance susceptibility by reducing overall C14 levels in the host apoplast. The execution of plant cell-autonomous immunity requires cytoskeleton reorganization and polarized secretion (25, 26). Although some bacterial effectors are known to target secretory pathways, little is known about the underlying cellular and molecular processes (27–29). The role of focal secretion in immunity has been difficult to dissect with standard genetic approaches because mutants often show pleiotropic effects that perturb plant development (26, 30). Our work indicates that effectors can be used as molecular probes to unravel unknown facets of focal immunity and potentially dissect the diversity of secretory vesicles and their cargo.

Our results implicate focal secretion of a plant defense protease in plant immunity. C14 could contribute to immunity by degrading non-self molecules or by playing a signaling role. C14 is known to accumulate during senescence and dehydration stress, but whether it also contributes to these processes is unclear (31, 32). During abiotic stress, C14 undergoes complex

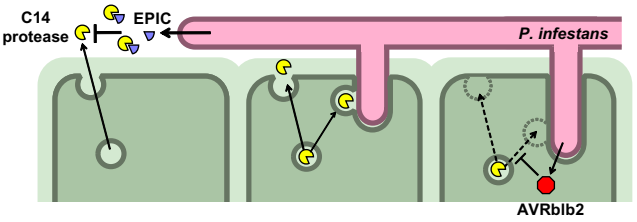

Fig. 6. Model of C14-EPIC-AVRblb2 interplay. C14 defense protease is secreted to the apoplast and inhibited by EPICs (5), which are secreted from growing *P. infestans* hyphae. Upon formation of haustoria, C14 is focally secreted to the extrahaustorial matrix. The RXLR effector AVRblb2 is translocated from *P. infestans* hyphae into the host cells and prevents secretion of C14.

changes in subcellular localization. It accumulates in atypical ER-derived vesicles and, upon dehydration stress, can directly traffic into the vacuole in a nonclassical way bypassing the Golgi pathway (16, 17). Also, during desiccation, C14 is released to the cytosol and nucleus (32). We showed that perturbation of C14 trafficking by *P. infestans* AVRblb2 limits its role in plant immunity. AVRblb2 association with C14 might occur directly or indirectly through an intermediate transmembrane protein or molecule. AVRblb2 could intercept C14 at various subcellular sites, including during release or fusion of secretory vesicles to the plasma membrane at the haustorial interface. Finally, our findings that C14 overexpression overcomes AVRblb2 activity and leads to enhanced resistance to *P. infestans* point to immediate biotechnological applications for engineering late blight-resistant potato and tomato crops.

Materials and Methods

Plasmid Construction. Effector expression constructs were designed to have N-terminal epitope or fluorescent tags replacing the native signal peptide to enable intracellular expression in plant cells. Detailed information about the plasmid constructs, transient gene-expression assays, and production of transgenic plants is described in *SI Materials and Methods*.

Co-IP Experiments. FLAG:AVRblb2 and its plant interactors were coimmunoprecipitated with anti-FLAG resins under nondenaturing conditions. Co-IP experiments, preparation of peptides for LC-MS/MS, and Western blot analysis are described in *SI Materials and Methods*.

Secretion Inhibition Assays. Secretion inhibition assays were performed by using *Agrobacterium*-mediated transient gene expression. Detailed procedures are provided in *SI Materials and Methods*.

Hypersensitive Response Cell-Death Assays. Hypersensitive response assays on C14 silencing are described in *SI Materials and Methods*.

RT-PCR Assays. Detailed RT-PCR procedures are explained in *SI Materials and Methods*.

Confocal Microscopy. Confocal microscopy analysis was performed on Leica DM6000B/TCS SP5 confocal microscope (Leica Microsystems). Detailed procedures of confocal microscopy and callose/aniline blue staining of infected material is described in *SI Materials and Methods*.

ACKNOWLEDGMENTS. We thank Ulla Bonas, Steve Whisson, and Frederick Boernke for providing biomaterials; Matthew Smoker, Liliya Serazetdinova, Jan Sklenář, and Richard O'Connell for technical advice and/or assistance; and Diane Saunders, Mireille van Damme, and Sylvain Raffaele for comments on drafts. This project was funded by the Gatsby Charitable Foundation; BASF Plant Science; Marie Curie Grant FP7-PEOPLE-2007-2-1-IEF; Deutsche Forschungsgemeinschaft Grants SCHO1347/1-1, HO 3983/7-1, and DAAD-HEC (Deutscher Akademischer Austausch Dienst and Higher Education Commission of Pakistan); and the Max Planck Society.

1. Panstruga R, Dodds PN (2009) Terrific protein traffic: The mystery of effector protein delivery by filamentous plant pathogens. *Science* 324:748–750.
2. Dodds PN, Rathjen JP (2010) Plant immunity: Towards an integrated view of plant–pathogen interactions. *Nat Rev Genet* 11:539–548.
3. Bednarek P, Kwon C, Schulze-Lefert P (2010) Not a peripheral issue: Secretion in plant–microbe interactions. *Curr Opin Plant Biol* 13:378–387.
4. Takemoto D, Hardham AR (2004) The cytoskeleton as a regulator and target of biotic interactions in plants. *Plant Physiol* 136:3864–3876.
5. Kaschani F, et al. (2010) An effector-targeted protease contributes to defense against *Phytophthora infestans* and is under diversifying selection in natural hosts. *Plant Physiol* 154:1794–1804.
6. Song J, et al. (2009) Apoplastic effectors secreted by two unrelated eukaryotic plant pathogens target the tomato defense protease Rcr3. *Proc Natl Acad Sci USA* 106: 1654–1659.
7. Bernoux M, et al. (2008) RD19, an *Arabidopsis* cysteine protease required for *RRS1-R*–mediated resistance, is relocalized to the nucleus by the *Ralstonia solanacearum* PopP2 effector. *Plant Cell* 20:2252–2264.
8. Haas BJ, et al. (2009) Genome sequence and analysis of the Irish potato famine pathogen *Phytophthora infestans*. *Nature* 461:393–398.
9. Tyler BM, et al. (2006) *Phytophthora* genome sequences uncover evolutionary origins and mechanisms of pathogenesis. *Science* 313:1261–1266.
10. Oh SK, et al. (2009) *in planta* expression screens of *Phytophthora infestans* RXLR effectors reveal diverse phenotypes, including activation of the *Solanum bulbocastanum* disease resistance protein Rpi-blb2. *Plant Cell* 21:2928–2947.
11. Schornack S, et al. (2009) Ten things to know about oomycete effectors. *Mol Plant Pathol* 10:795–803.
12. Bos JI, et al. (2010) *Phytophthora infestans* effector AVR3a is essential for virulence and manipulates plant immunity by stabilizing host E3 ligase CMPG1. *Proc Natl Acad Sci USA* 107:9909–9914.
13. Whisson SC, et al. (2007) A translocation signal for delivery of oomycete effector proteins into host plant cells. *Nature* 450:115–118.
14. van Damme M, et al. (2009) Downy mildew resistance in *Arabidopsis* by mutation of *HOMOSERINE KINASE*. *Plant Cell* 21:2179–2189.
15. Avrova AO, et al. (1999) A cysteine protease gene is expressed early in resistant potato interactions with *Phytophthora infestans*. *Mol Plant Microbe Interact* 12: 1114–1119.
16. Hayashi Y, et al. (2001) A proteinase-storing body that prepares for cell death or stresses in the epidermal cells of *Arabidopsis*. *Plant Cell Physiol* 42:894–899.
17. Yamada K, Matsushima R, Nishimura M, Hara-Nishimura I (2001) A slow maturation of a cysteine protease with a granulin domain in the vacuoles of senescing *Arabidopsis* leaves. *Plant Physiol* 127:1626–1634.
18. Shabab M, et al. (2008) Fungal effector protein AVR2 targets diversifying defense-related cys proteases of tomato. *Plant Cell* 20:1169–1183.
19. Pechan T, et al. (1999) Characterization of three distinct cDNA clones encoding cysteine proteinases from maize (*Zea mays* L.) callus. *Plant Mol Biol* 40:111–119.
20. Watanabe H, Abe K, Emori Y, Hosoyama H, Arai S (1991) Molecular cloning and gibberellin-induced expression of multiple cysteine proteinases of rice seeds (oryzains). *J Biol Chem* 266:16897–16902.
21. Shindo T, Van der Hoorn RA (2008) Papain-like cysteine proteases: Key players at molecular battlefields employed by both plants and their invaders. *Mol Plant Pathol* 9:119–125.
22. Tian M, Benedetti B, Kamoun S (2005) A Second Kazal-like protease inhibitor from *Phytophthora infestans* inhibits and interacts with the apoplastic pathogenesis-related protease P69B of tomato. *Plant Physiol* 138:1785–1793.
23. Jones JD, Dangl JL (2006) The plant immune system. *Nature* 444:323–329.
24. van der Hoorn RAL, Kamoun S (2008) From Guard to decoy: A new model for perception of plant pathogen effectors. *Plant Cell* 20:2009–2017.
25. Hardham AR, Jones DA, Takemoto D (2007) Cytoskeleton and cell wall function in penetration resistance. *Curr Opin Plant Biol* 10:342–348.
26. Kwon C, et al. (2008) Co-option of a default secretory pathway for plant immune responses. *Nature* 451:835–840.
27. Bartetzko V, et al. (2009) The *Xanthomonas campestris* pv. vesicatoria type III effector protein XopJ inhibits protein secretion: Evidence for interference with cell wall-associated defense responses. *Mol Plant Microbe Interact* 22:655–664.
28. Kaffarnik FA, Jones AM, Rathjen JP, Peck SC (2009) Effector proteins of the bacterial pathogen *Pseudomonas syringae* alter the extracellular proteome of the host plant, *Arabidopsis thaliana*. *Mol Cell Proteomics* 8:145–156.
29. Tian M, et al. (2009) *Arabidopsis* actin-depolymerizing factor AtADF4 mediates defense signal transduction triggered by the *Pseudomonas syringae* effector AvrPphB. *Plant Physiol* 150:815–824.
30. Sup Yun H, Panstruga R, Schulze-Lefert P, Kwon C (2008) Ready to fire: Secretion in plant immunity. *Plant Signal Behav* 3:505–508.
31. Drake R, et al. (1996) Isolation and analysis of cDNAs encoding tomato cysteine proteases expressed during leaf senescence. *Plant Mol Biol* 30:755–767.
32. Harrak H, Azelmat S, Baker EN, Tabaeizadeh Z (2001) Isolation and characterization of a gene encoding a drought-induced cysteine protease in tomato (*Lycopersicon esculentum*). *Genome* 44:368–374.

Supporting Information

Bozkurt et al. 10.1073/pnas.1112708109

SI Materials and Methods

Plasmid Construction. All of the primers used in this study are available on request. *FLAG:Avrblb2*, *FLAG:Avr3a*, and *FLAG:RFP* constructs were custom-synthesized with the signal peptide regions removed (GenScript Corp.) and subcloned into the *tobacco mosaic virus*-based *Agrobacterium tumefaciens* binary vector pTRBO (1). The tomato C14 expression construct (pFK26::*C14*) and tomato P69B construct (pBinPlus::P69B) used in this study were described elsewhere (2, 3). Data mining to identify the C14 domains was achieved with the MEROPS database of proteases (http://merops.sanger.ac.uk/) and PFAM (http://pfam.janelia.org/).

Avrblb2 was cloned into pDNOR207 (Invitrogen) by Gateway BP recombination reaction (Invitrogen) with the PCR products amplified by using pTRBO::*FLAG:Avrblb2* as a template and RD39/40-F + RD39/40-R as primers. GFP and RFP fusions of *Avrblb2* were generated by Gateway LR recombination (Invitrogen) of pDONR207::*Avrblb2* and pK7WGF2 (*GFP:Avrblb2*) or pGWB555 (*RFP:Avrblb2*) (4, 5). *C14pep:GFP* and *C14pep:RFP* fusions were generated by cloning *C14* peptidase PCR amplicons produced by using pFK26::*C14* as a template with C14-FL-F/C14PepR_GW-TB primers into pENTR/D-TOPO (Invitrogen) followed by Gateway LR recombination (Invitrogen) into pK7FWG2 or pGWB554. *C14:GFP* and *C14:RFP* constructs were generated by cloning PCR amplicons produced by using pFK26::*C14* as a template with C14-FL-F + C14-FL-YFP-R primers into pENTR/D-TOPO (Invitrogen) followed by Gateway LR recombination (Invitrogen) into pK7FWG2 or pGWB554. *GFP:Avrblb2*$^{47–100}$ and *GFP:Avrblb2*$^{47–92}$ were generated by cloning PCR amplicons produced by using primer pairs Rd40_F + Rd40_R and Rd40_F + C2D_R into pENTR/D-TOPO (Invitrogen) followed by Gateway LR recombination (Invitrogen) into pK7WGF2. The *GFP:3xHA* construct and the subcellular marker constructs plasma membrane-localized CFP (pmC) and endoplasmic reticulum (ER)-CFP were described previously (5, 6).

Hairpin-silencing constructs of *Nicotiana benthamiana C14-1* (pTS54) and *C14-2* (pTS55) were described by Kaschani et al. (7). All of the mentioned vector constructs were transformed into *A. tumefaciens* GV3101 strain by electroporation.

Transgenic *N. benthamiana* Lines. Multiple transgenic *N. benthamiana* lines stably expressing *GFP:Avrblb2* or *C14pep:RFP* were generated as described elsewhere (8) with the pK7WGF2::*Avrblb2* and pGWB554::*C14pep* constructs, respectively. *C14* knockdown *N. benthamiana* lines were generated by using pTS54 and pTS55 constructs.

Transient Gene-Expression Assays. *A. tumefaciens*-mediated transient expression (agroinfiltration) experiments were performed on 4- to 6-wk-old *N. benthamiana* plants. Plants were grown and maintained throughout the experiments in a greenhouse with an ambient temperature of 22–25 °C and high light intensity. *in planta* transient expression by agroinfiltration was performed according to methods described previously (9). For each of the *A. tumefaciens* strains, a final OD_{600} of 0.3–0.4 in agroinfiltration medium [10 mM MES, 10 mM $MgCl_2$, and 150 μM acetosyringone (pH 5.6)] was used. For all of the transient coexpression assays, *A. tumefaciens* strains carrying the plant expression constructs were mixed in a 1:1 ratio in agroinfiltration medium to a final OD_{600} of 0.4–0.6.

Coimmunoprecipitation (Co-IP) Experiments and LC-MS/MS Analysis. For co-IP experiments, total proteins were extracted from *N. benthamiana* leaves at 3 d after agroinfiltration of pTRBO::*FLAG:Avrblb2* or pTRBO::*FLAG:RFP* constructs and subjected to immunoprecipitation as described previously (10).

Preparation of peptides for liquid chromatography–tandem mass spectrometry (LC-MS/MS) was performed as follows. Proteins were separated with SDS/PAGE. Gels were cut into slices (~5 × 10 mm). Proteins contained in gel slices were prepared for LC-MS/MS as described previously (11). LC-MS/MS analysis was performed with a LTQ Orbitrap mass spectrometer (Thermo Scientific) and a nanoflow-HPLC system (nanoACQUITY; Waters Corp.) as described previously (12) with the following differences: MS/MS peak lists were exported in mascot generic file format by using Discoverer v2.2 (Thermo Scientific).

The database was searched with Mascot v2.3 (Matrix Science) with the following differences: (*i*) The database searched with Mascot v2.3 (Matrix Science) was against a custom collection of translated sequences from transcript assemblies (TIGR Plant Transcript Assemblies; http://plantta.jcvi.org) of solanaceous plants (*Solanum lycopersicum*, *N. benthamiana*, *Nicotiana tabacum*, *Solanum tuberosum*, *Capsicum annuum*, and *Petunia hybrida*) and *Phytophthora infestans* sequences containing 1,000,691 sequences (98,308,278 amino acid residues) with the inclusion of sequences of common contaminants such as keratins and trypsin. (*ii*) Carbamidomethylation of cysteine residues was specified as a fixed modification, and oxidized methionine was allowed as a variable modification.

Other Mascot parameters used were as follows: (*i*) Mass values were monoisotopic, and the protein mass was unrestricted. (*ii*) The peptide mass tolerance was 5 ppm, and the fragment mass tolerance was ± 0.6 Da. (*iii*) Two missed cleavages were allowed with trypsin. All Mascot searches were collated and verified with Scaffold (Proteome Software), and the subset database was searched with X! Tandem (The Global Proteome Machine Organization Proteomics Database and Open Source Software; www.thegpm.org). Accepted proteins passed the following threshold in Scaffold: 95% confidence for protein match and minimum of two unique peptide matches with 95% confidence.

To validate the *in planta* association of AVRblb2 and C14, co-IP assays were performed as follows. *FLAG:Avrblb2*, *FLAG:Avr3a*, or *FLAG:RFP pTRBO* constructs were transiently coexpressed in *N. benthamiana* with pFK26::*C14* by agroinfiltration followed by extraction of proteins.

Western Blot Analysis. Western blot analyses were performed on SDS/PAGE-separated proteins as described elsewhere (12). Monoclonal FLAG M2 antibodies and polyclonal GFP antibodies were obtained from Sigma and Invitrogen, respectively. C14 antisera (2) were raised in rabbits with peptides DTEEDYPYKERNGVC and DQYRKNAKVVKIDSYC (Eurogentec).

Secretion Inhibition Assays. Independent secretion inhibition experiments were executed by using *pTRBO::FLAG:Avrblb2* or *pTRBO::FLAG:RFP* as well as the *A. tumefaciens* binary constructs of *GFP:Avrblb2* or *GFP:3xHA* (under the control of the *cauliflower mosaic virus* 35S promoter). Secretion inhibition assays were performed by agroinfiltration of *Avrblb2* or *RFP/GFP* constructs (OD_{600} of 0.3) followed by agroinfiltration of *C14* or *P69B* (OD_{600} of 0.3) together with P19 (OD_{600} of 0.1) silencing suppressor construct at 24 h after the first set of infiltrations. Apoplastic fluids were extracted as described elsewhere (2) at 3

d after the first agroinfiltrations. Intracellular proteins were extracted from the remaining leaf pellets that were used for apoplastic fluid isolation.

The effect of AVRblb2 on C14pep:RFP secretion was also addressed with imaging of confocal planes of *N. benthamiana* epidermal cells and apoplast after initial *A. tumefaciens*-mediated expression of *GFP:Avrblb2* followed 1 d later by agroinfiltration of *C4pep:RFP*. Confocal settings were as described below, and multipass scanning was used to prevent bleed-through.

To study whether AVRblb2 inhibits secretion of other proteins, a fusion of basic chitinase signal peptide to *GFP* (*SP:GFP*) (13) was coexpressed in *N. benthamiana* together with 35S-*XopJ* (13), *FLAG:Avrblb2*, or *FLAG:RFP* by agroinfiltration.

Secretion inhibition assay during *P. infestans* colonization on tomato was performed as follows. After spray-inoculation of *P. infestans* 88069 zoospores (10,000 zoospores per mL) on tomato leaves, apoplastic fluids and intracellular proteins were extracted at time points 0, 6, 12, 24, 48, and 72 h after inoculation. Immunoblot analyses were performed as described above.

Hypersensitive Response Cell-Death Assays. *A. tumefaciens* strains carrying short hairpin-silencing constructs (pTP5-hpC14-1 and pTP5-hpC14-2) of *NbC14-1* and *NbC14-2* were infiltrated into *N. benthamiana* leaves (whole leaf surface) stably expressing the *Rpi-blb2* resistance gene, either individually or by mixing both strains in a 1:1 ratio to a final OD_{600} of 0.3 in induction buffer [10 mM $MgCl_2$, 5 mM MES (pH 5.3), and 150 μM acetosyringone]. pTP5 empty vector was used as a control for the hypersensitive response assay. At 2 d after delivery of silencing constructs, *A. tumefaciens* strains harboring the binary expression constructs *GFP:Avrblb2*, *GFP*, or p35S-*Inf1* (9) were infiltrated on each silenced leaf panel. *Rpi-blb2*–mediated hypersensitive response cell death was monitored at 4 d after *GFP:Avrblb2* expression.

RT-PCR Assays. For transient C14 silencing and *Rpi-blb2*–mediated hypersensitive response assays, total RNA was extracted according to the manufacturer's protocol (Qiagen) with 100 mg of leaf samples collected from each C14-silenced and control *N. benthamiana* leaves at 6 d after silencing. For selection of C14 knockdown lines, 100-mg leaf samples were collected from 6-wk-old *N. benthamiana* transgenic plants, and total RNA was extracted as described above. Extracted total RNAs (10 mg) were subjected to DNase I treatment (Ambion) according to the manufacturer's protocol. cDNA was generated with 1 μg of DNase-treated RNA and diluted to a 1:5 ratio for PCR. Primer combinations Nbrd21-F-TB + Nbrd21-R-TB and Nbrd21-F2-TB + Nbrd21-R2-TB were used to detect *NbC14-1* and *NbC14-2* transcripts. *GAPDH* was used as a control for RT-PCR analysis and amplified with primers SILG3PF-TB + SILG3PR-TB.

Pathogenicity Assays. *P. infestans* infection assays on *N. benthamiana* were performed by droplet inoculations of zoospore solutions on detached leaves as described earlier (14, 15). Pathogenicity assays on *N. benthamiana* transgenic lines stably expressing *GFP:Avrblb2* and control plants that express an ER-localized GFP (16c) were performed as follows: Detached leaves (5 wk old) were challenged with *P. infestans* isolates 88069 (50,000 zoospores per mL) and 88069td (100,000 zoospores per mL) on six different spots. *P. infestans* hyphal growth was monitored by using confocal microscopy at 2–4 d postinfection (dpi), and infection phenotypes were scored at 6 dpi. Infection phenotypes were scored as lesions of necrotic growth, sporulation, or no visible growth. Successful infections at each *Phytophthora*-inoculated spot were used to analyze the growth efficiency. The assay was repeated at least three times, and a representative dataset is used. Pathogenicity assays on C14-knockdown *N. benthamiana* transgenic lines (10 wk old) were performed similarly with the *P. infestans* isolate 88069.

Infection assays assessing the effect of C14 overexpression on disease were performed as follows. First, *C14:GFP* (or *C14pep:GFP*) and *GFP* were transiently overexpressed side by side on either halves of four independent *N. benthamiana* leaves (4 wk old) by *A. tumefaciens*-mediated transient expression. At 48 h postinfection, the infiltrated leaves were detached and inoculated with 88069td on three spots for each leaf half. *P. infestans* hyphal growth was monitored by using confocal microscopy at 5 dpi. The growth efficiency was quantified by measuring the total area of the red fluorescent hyphae for each inoculated spot with the ImageJ program (National Institutes of Health; http://rsbweb.nih.gov/ij). An average growth value for each leaf was used to generate the histograms.

Transgenic *N. benthamiana* plants (5 wk old) stably expressing *C14pep:RFP* were first selected by examining RFP fluorescence with confocal microscopy. Pathogenicity assays on these lines were performed with *P. infestans* 88069 zoospores as described above, and phenotypes were scored at 6 dpi.

Pathogenicity assays to test the extent to which AVRblb2 circumvents the enhanced resistance conferred by C14 were performed as follows. Combinations of *RFP:Avrblb2*, *C14:GFP*, *GFP*, and *RFP* were expressed in *N. benthamiana* leaves (5 wk old) by *A. tumefaciens*-mediated transient expression. *P. infestans* zoospore suspensions (three droplets per treatment) were applied at 24 h postinfiltration on 15 expressing leaf patches per construct. Then, 3 d later, infection phenotypes were scored with UV illumination, and autofluorescent spots were counted.

Confocal Microscopy. Patches of *N. benthamiana* leaves were cut and mounted in water and analyzed on a Leica DM6000B/TCS SP5 confocal microscope (Leica Microsystems) with the following excitation wavelengths: CFP, 458 nm; GFP, 488 nm; and RFP, 561 nm. Scanning was performed in sequential mode to prevent signal bleed-through. Identical microscope settings were applied for all individual images shown in a given figure to allow comparison of fluorescence intensities between samples.

Callose/Aniline Blue Staining of Infected Material. *P. infestans*-infected leaf material was rinsed twice with 50% ethanol and once with 0.07 M phosphate buffer (pH 9.0). After incubation for 30 min in 0.07 M phosphate buffer (pH 9.0) at room temperature, the buffer was replaced by freshly prepared 0.05% aniline blue (wt/vol in 0.07 M phosphate buffer), and samples were incubated for 60 min in the dark. Samples were mounted on slides in 0.05% aniline blue and imaged with UV illumination.

1. Lindbo JA (2007) TRBO: A high-efficiency tobacco mosaic virus RNA-based overexpression vector. *Plant Physiol* 145:1232–1240.
2. Shabab M, et al. (2008) Fungal effector protein AVR2 targets diversifying defense-related cys proteases of tomato. *Plant Cell* 20:1169–1183.
3. Tian M, Benedetti B, Kamoun S (2005) A Second Kazal-like protease inhibitor from *Phytophthora infestans* inhibits and interacts with the apoplastic pathogenesis-related protease P69B of tomato. *Plant Physiol* 138:1785–1793.
4. Karimi M, Inzé D, Depicker A (2002) GATEWAY vectors for *Agrobacterium*-mediated plant transformation. *Trends Plant Sci* 7:193–195.
5. Nakagawa T, et al. (2007) Improved Gateway binary vectors: High-performance vectors for creation of fusion constructs in transgenic analysis of plants. *Biosci Biotechnol Biochem* 71:2095–2100.
6. Nelson BK, Cai X, Nebenführ A (2007) A multicolored set of in vivo organelle markers for co-localization studies in *Arabidopsis* and other plants. *Plant J* 51:1126–1136.
7. Kaschani F, et al. (2010) An effector-targeted protease contributes to defense against *Phytophthora infestans* and is under diversifying selection in natural hosts. *Plant Physiol* 154:1794–1804.
8. Horsch RB, et al. (1985) A simple and general method for transferring genes into plants. *Science* 227:1229–1231.
9. Bos JI, et al. (2006) The C-terminal half of *Phytophthora infestans* RXLR effector AVR3a is sufficient to trigger R3a-mediated hypersensitivity and suppress INF1-induced cell death in *Nicotiana benthamiana*. *Plant J* 48:165–176.
10. Rairdan GJ, Moffett P (2006) Distinct domains in the ARC region of the potato resistance protein Rx mediate LRR binding and inhibition of activation. *Plant Cell* 18:2082–2093.

11. Ntoukakis V, et al. (2009) Host inhibition of a bacterial virulence effector triggers immunity to infection. *Science* 324:784–787.
12. Oh SK, et al. (2009) *in planta* expression screens of *Phytophthora infestans* RXLR effectors reveal diverse phenotypes, including activation of the *Solanum bulbocastanum* disease resistance protein Rpi-blb2. *Plant Cell* 21:2928–2947.
13. Bartetzko V, et al. (2009) The *Xanthomonas campestris* pv. *vesicatoria* type III effector protein XopJ inhibits protein secretion: Evidence for interference with cell wall-associated defense responses. *Mol Plant Microbe Interact* 22:655–664.
14. Song J, et al. (2009) Apoplastic effectors secreted by two unrelated eukaryotic plant pathogens target the tomato defense protease Rcr3. *Proc Natl Acad Sci USA* 106: 1654–1659.
15. Kamoun S, Huitema E, Vleeshouwers VG (1999) Resistance to oomycetes: A general role for the hypersensitive response? *Trends Plant Sci* 4:196–200.

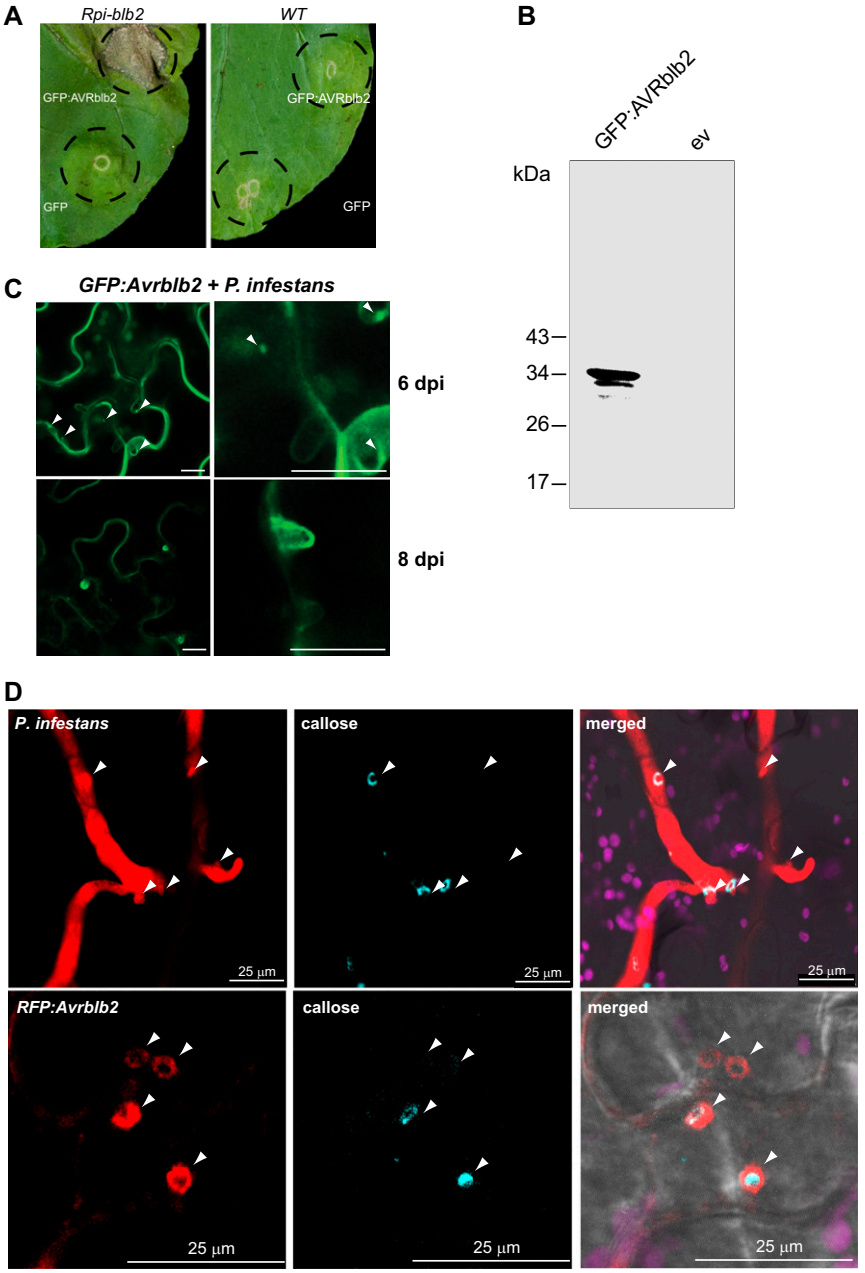

Fig. S1. GFP:AVRblb2 localizes at haustoria in *P. infestans*-infected cells. (*A*) Symptoms observed upon *A. tumefaciens*-mediated transient expression of *GFP:Avrblb2* or *GFP* in transgenic *N. benthamiana* leaves stably expressing *Rpi-blb2* (*Left*) or WT (*Right*) at 5 d after agroinfiltration. (*B*) GFP:AVRblb2 is a stable fusion protein in *N. benthamiana*. (*C*) GFP:AVRblb2 accumulation at haustoria is initiated at focal spots (arrowheads) in stable transgenic *GFP:Avrblb2 N. benthamiana* lines infected with *P. infestans* strain 88069. (Scale bars: 5 μm.) (*D*) Haustoria (arrowheads) are not surrounded by callose (papillae) encasements. *P. infestans* 88069td-infected *N. benthamiana* leaves (red) were stained with aniline blue at 5 d after inoculation and revealed callosic deposition only in haustorial neckbands (cyan). For 50% of haustoria, no callose was detectable by aniline blue staining. Aniline blue staining of leaf patches transiently expressing *RFP:Avrblb2* and infected with *P. infestans* isolate 88069 showed that AVRblb2 haustorial accumulation is not attributable to papillae encasements (*Lower*). Plastid autofluorescence is shown in magenta in merged panels.

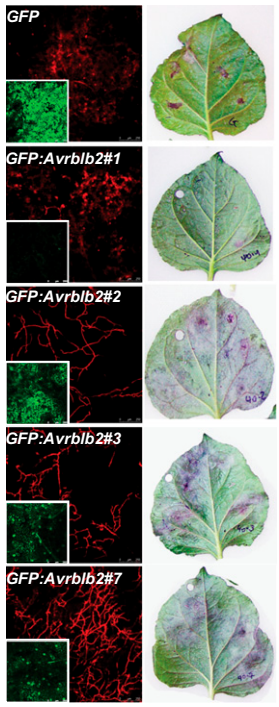

Fig. S2. GFP:AVRblb2 transgenic *N. benthamiana* plants display enhanced susceptibility to *P. infestans* infection. Descendants of four independent transgenic lines (5 wk old) with different GFP:AVRblb2 levels as assessed by GFP fluorescence (*Insets*) were challenged with *P. infestans* isolates 88069 and 88069td. *P. infestans* hyphal growth was monitored by using confocal microscopy at 2–4 d post infection (*Left*) and infection phenotypes at 6 d post infection (*Right*). We observed intensified hyphal growth and a significantly higher proportion of infection sites with lesions and sporulation in plants expressing *GFP:AVRblb2* (*Right*) compared with control plants that express *GFP* (line 16c, first row). *GFP:Avrblb2*#1 descendants without detectable GFP:AVRblb2 levels showed similar levels of infection to those of control plants.

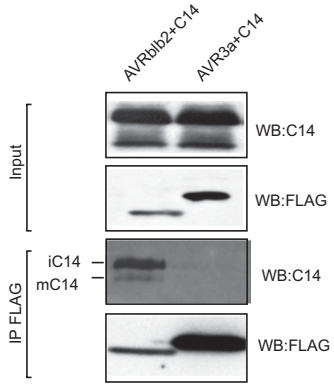

Fig. S3. AVRblb2 associates with both immature (iC14) and mature (mC14) *in planta*. *FLAG:Avrblb2* was coexpressed with *C14 in planta* by *A. tumefaciens*-mediated transient expression and subjected to FLAG immunoprecipitation. *FLAG:Avr3a* coexpressed with *C14* was used as a negative control. Purified immunocomplexes were analyzed by immunoblotting to identify association of coexpressed proteins with anti-C14 and anti-FLAG antibodies (IP FLAG). Two bands representing iC14 (~37 kDa) and mC14 (~30 kDa) were detected in complex with AVRblb2 but not with AVR3a.

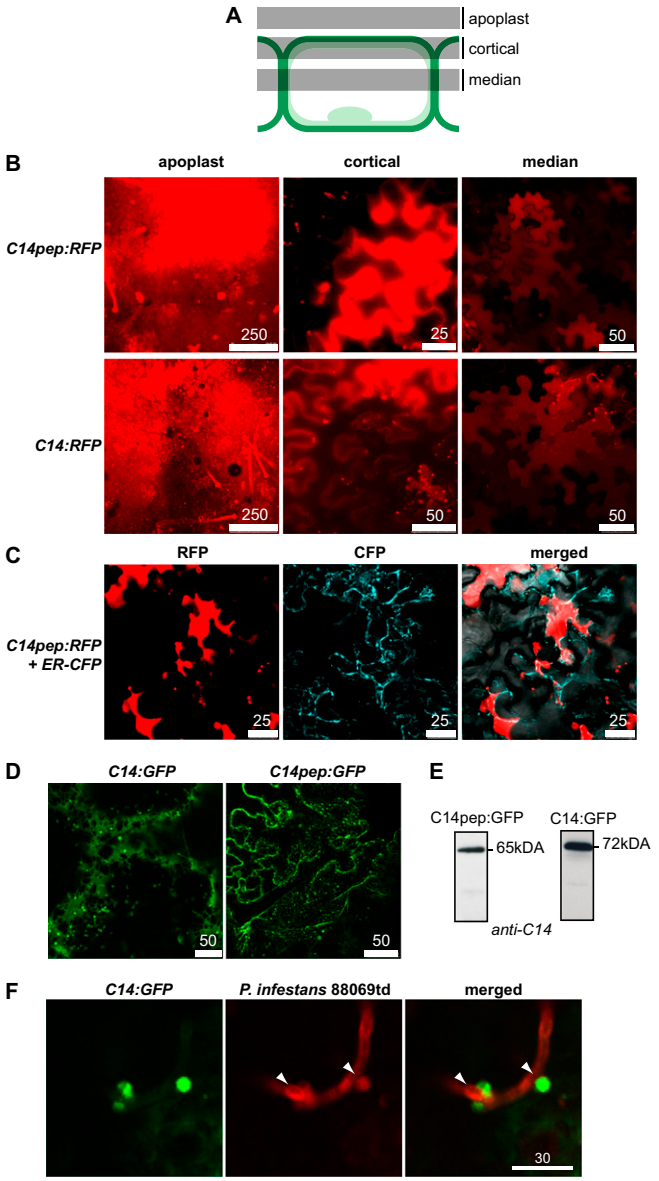

Fig. S4. Cellular localization of C14 and C14pep proteins. (*A*) Confocal sections of *N. benthamiana* epidermis were analyzed for localization of C14 that was expressed using *A. tumefaciens*-mediated transient assays. (*B*) RFP fusions of C14 and C14pep were detected in the apoplast, intercellular spaces and the central vacuole at 2 d post infiltration. (*C*) Plasmolysis of *C14pep:RFP*- and *ER-CFP*–expressing cells showed shrinking vacuoles labeled with red fluorescent C14pep. (*D*) To specifically trace C14 localization inside the secretory pathway, we transiently expressed *GFP* fusions of *C14* or *C14pep*, given that GFP is not fluorescent under apoplastic or vacuolar pH conditions and therefore enables visualization of secretory membrane compartments. Confocal microscopy revealed distribution in endomembrane compartments and networks typical of the ER for both constructs. (*E*) Presence of intact C14pep:GFP or C14:GFP fusion proteins in protein extracts of *N. benthamiana* leaves transiently expressing the protease constructs with C14 antisera. (*F*) Confocal imaging of transiently expressed C14:GFP, which accumulates around haustoria (arrowheads) of *P. infestans* 88069td (RFP) at 4 dpi.

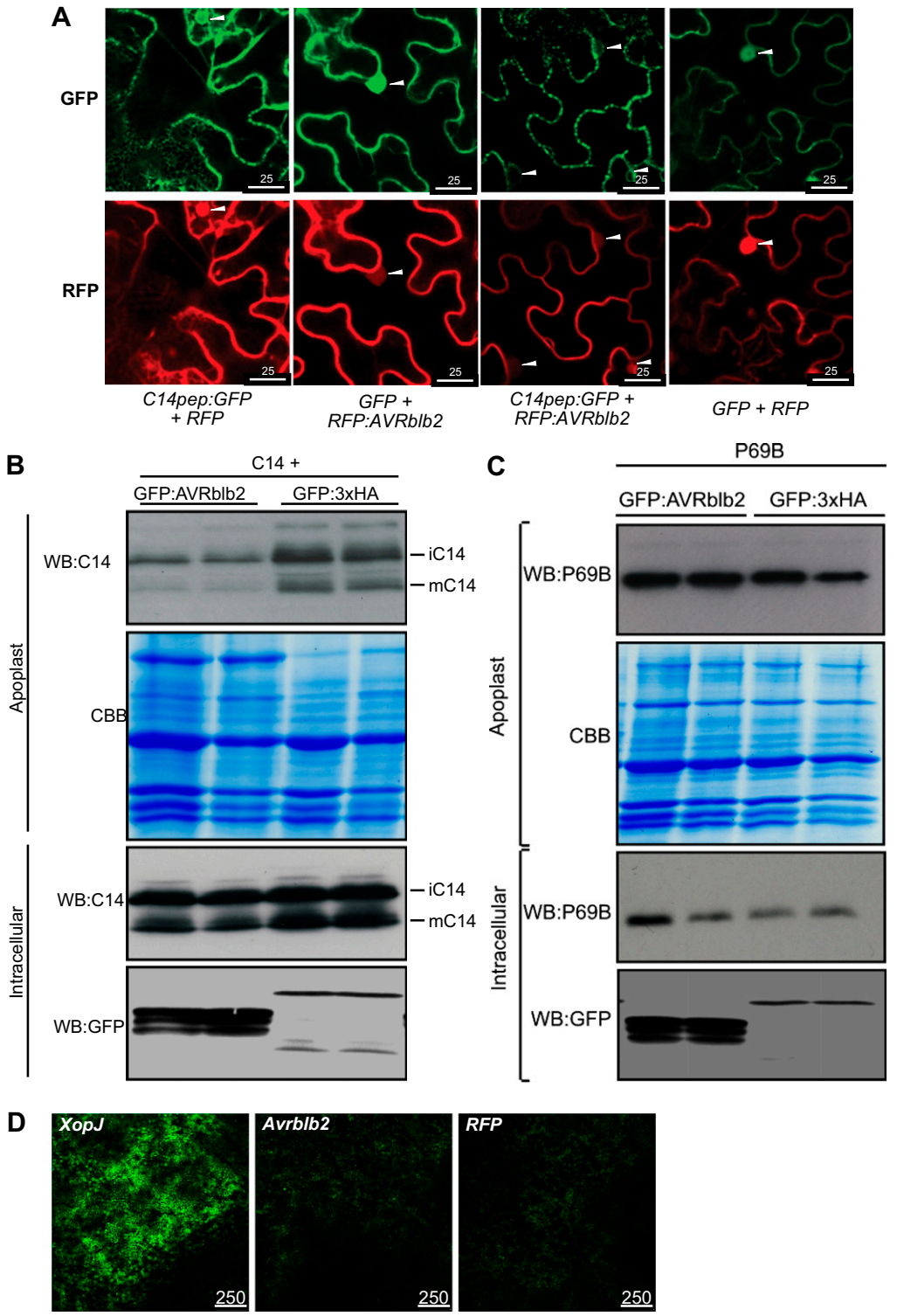

Fig. S5. AVRblb2 alters trafficking of C14. (*A*) Confocal microscopy revealed that RFP:AVRblb2 localization was not affected by *A. tumefaciens*-mediated transient coexpression of *C14:GFP* and remained peripheral and weakly nuclear in *N. benthamiana*. Transient expression of *C14:GFP* with the *RFP* control resulted in an ER-like distribution of the C14:GFP fusion protein (*First column*). However, coexpression of *RFP:Avrblb2* and *C14:GFP* resulted in an increased amount of peripheral small endomembrane compartments for the C14:GFP fusion (*Third column*). Arrowheads mark nuclei. (Bars: 25 μm.) (*B*) GFP:AVRblb2 inhibits the secretion of C14. *GFP:Avrblb2* or *GFP* constructs were transiently coexpressed with *C14* in *N. benthamiana* leaves (two independent leaves for each construct). Apoplastic and intracellular extracts from infiltrated leaves were separated followed by Coomassie Brilliant Blue (CBB) staining and immunoblotting. (*C*) GFP:AVRblb2 does not inhibit the secretion of the pathogenesis-related protein P69B. (*D*) AVRblb2 does not inhibit the secretion of SP:GFP. Transient expression of *SP-GFP* with *pTRBO::FLAG:RFP* and *pTRBO::FLAG:Avrblb2* did not result in gain of fluorescence, whereas 35S-*XopJ* expression resulted in intracellular retention of secreted GFP as previously reported (1). (Bars: 250 μm.)

1. Bartetzko V, et al. (2009) The *Xanthomonas campestris* pv. *vesicatoria* type III effector protein XopJ inhibits protein secretion: Evidence for interference with cell wall-associated defense responses. *Mol Plant Microbe Interact* 22:655–664.

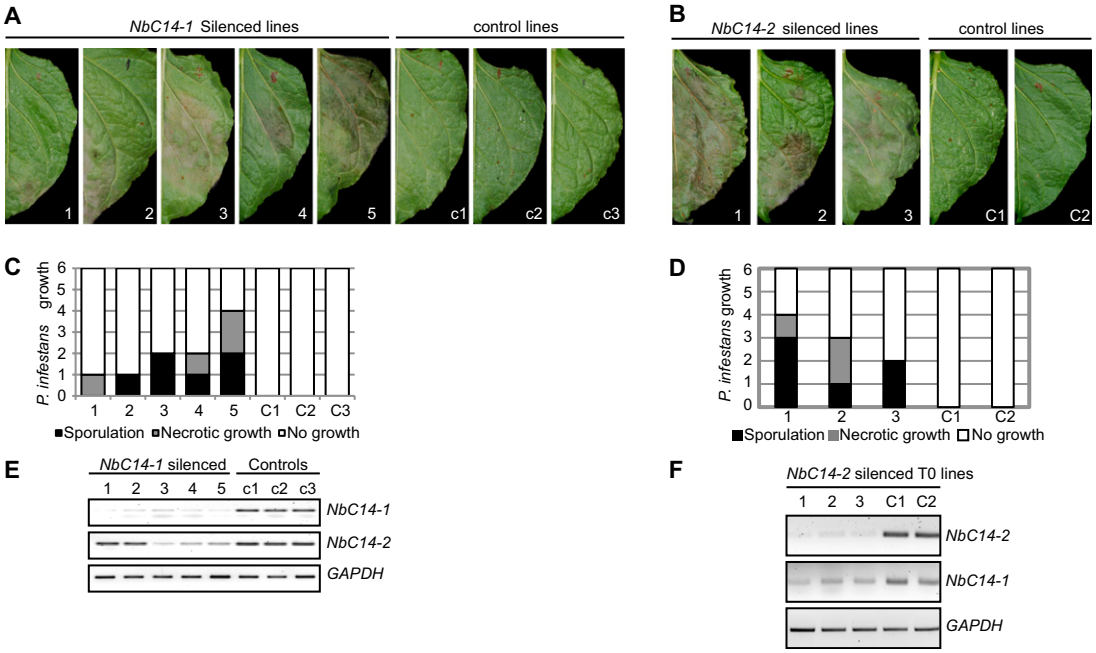

Fig. S6. Silencing of *NbC14-1* increases susceptibility to *P. infestans*. (*A*) Differential colonization of *P. infestans* 88069 on *NbC14-1* silenced and nonsilenced *N. benthamiana* transgenic lines (10 wk old). Pictures were taken at 6 d postinfection (dpi). (*B*) A histogram depicting the enhanced virulence of *P. infestans* on *C14* silenced lines shown in *A*. Symptoms were scored at 6 dpi by monitoring *P. infestans* growth on each inoculation spot (six different spots per leaf). (*C*) Validation of *C14* silencing by RT-PCR in the plants described in *A*. (*D*) Promoted growth of *P. infestans* on *NbC14-2* silenced versus nonsilenced *N. benthamiana* transgenic lines (10 wk old) transformed with binary constructs of pTP5-hpC14-2. *NbC14-2* silenced and control lines were infected with droplet inoculations of *P. infestans* zoospores at six different spots on each leaf. Pictures were taken at 6 dpi. (*E*) Histogram depicting the enhanced virulence of *P. infestans* on the *C14* silenced lines described in *D*. Symptoms were scored at 6 dpi by monitoring *P. infestans* growth on each inoculation spot. (*F*) Validation of *C14* silencing by RT-PCR in plants described in *D*.

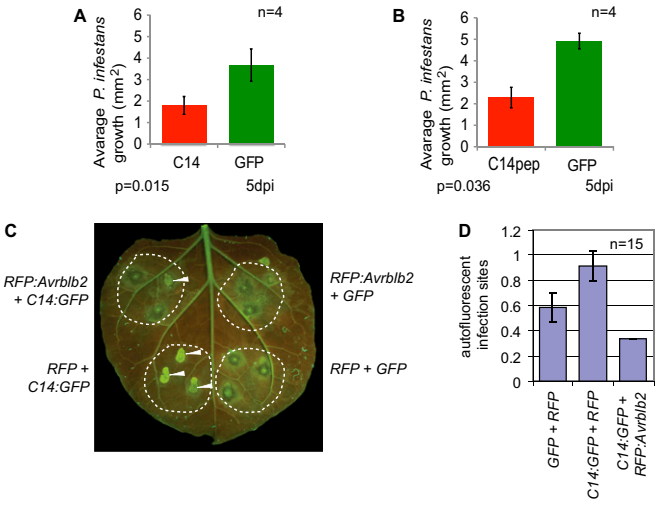

Fig. S7. AVRblb2 can circumvent enhanced resistance mediated by C14. (*A* and *B*) *A. tumefaciens*-mediated transient overexpression of *C14:GFP* (*A*) or *C14pep:GFP* (*B*) but not *GFP* in 5-wk-old *N. benthamiana* limits *P. infestans* 88069td growth. *P. infestans* isolate 88069td spore suspension (three droplets per expression) was applied at 24 h postinfiltration; 3 d later, infection phenotypes where scored with UV illumination. (*C*) AVRblb2 can overcome enhance resistance mediated by C14. Combinations of *RFP:Avrblb2*, *C14:GFP*, *GFP*, and *RFP* in *N. benthamiana* (5 wk old) were expressed by *A. tumefaciens*-mediated transient expression (agroinfiltration). *P. infestans* 88069 spore suspension (three droplets per expression) was applied at 24 h postinfiltration; 3 d later, infection phenotypes where scored with UV illumination. Autofluorescent spots (arrowheads) indicate an early partial defense response. (*D*) Frequency (with SD) of fluorescent spots in 15 leaves as observed at 3 d after transient expression of given constructs.

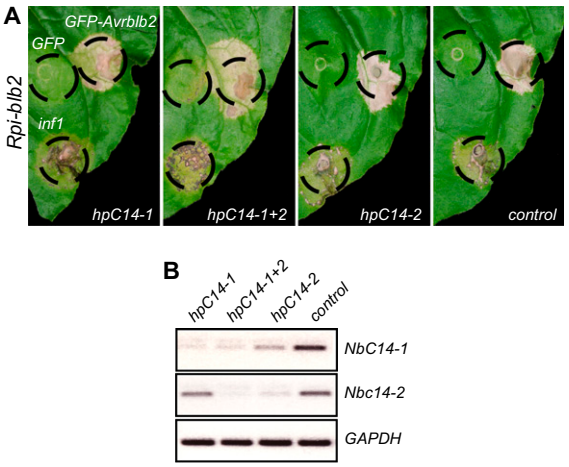

Fig. S8. *C14* is not required for *Rpi-blb2*–mediated hypersensitive response cell death. (*A*) Symptoms observed in *NbC14* silenced and control leaves upon *in planta* expression of *Avrblb2*, *Inf1* (positive cell-death control), or *GFP* (negative control) constructs. *C14* silencing constructs hpC14-1 and hpC14-2 were expressed alone or together by *A. tumefaciens*-mediated transient expression (agroinfiltration) in *N. benthamiana* plants carrying *Rpi-blb2*. Empty vector was used as a negative control. *GFP:Avrblb2*, *GFP*, or *Inf1* was expressed in *N. benthamiana C14* silenced and control leaves at 4 d after transient silencing by agroinfiltration. Pictures were taken at 5 d postinfiltration (dpi) of *Avrblb2* or control constructs. (*B*) Verification of *C14* silencing by RT-PCR.

Table S1. Plant proteins that associate specifically with AVRblb2 *in planta*

Identified protein	Description	Accession no.	No. of unique peptides		
			Sample 1	Sample 2	Sample 3
C14	Papain-like cysteine protease (PLCP)	TC9688*	4	2	4
Proteinase inhibitor	Similar to *S. tuberosum* proteinase inhibitor I	TC8657*	0	2	0
Cystatin	Cysteine protease inhibitor	DV105642†	1	1	3
GrpE	Chaperone	Q03685†	4	0	2
BiP 5	Chaperone	AF098635†	17	2	26

*Tobacco sequence accession no. from the Dana-Farber Cancer Institute *N. tabacum* Gene Index (http://compbio.dfci.harvard.edu/tgi/plant.html). GrpE, glucose regulated protein E; BiP 5, binding immunoglobulin protein 5.
†GenBank accession no.